JACS
JOURNAL OF THE AMERICAN CHEMICAL SOCIETY
Article
pubs.acs.org/JACS

Sintering-Resistant Single-Site Nickel Catalyst Supported by Metal–Organic Framework

Zhanyong Li,[†] Neil M. Schweitzer,[†] Aaron B. League,[‡] Varinia Bernales,[‡] Aaron W. Peters,[†] Andrew "Bean" Getsoian,[§] Timothy C. Wang,[†] Jeffrey T. Miller,[§,∥] Aleksei Vjunov,[⊥] John L. Fulton,[⊥] Johannes A. Lercher,[⊥,#] Christopher J. Cramer,*[,‡] Laura Gagliardi,*[,‡] Joseph T. Hupp,*[,†] and Omar K. Farha*[,†,¶]

[†]Department of Chemistry and Chemical and Biological Engineering, Northwestern University, 2145 Sheridan Road, Evanston, Illinois 60208, United States

[‡]Department of Chemistry, Supercomputing Institute, and Chemical Theory Center, University of Minnesota, Minneapolis, Minnesota 55455, United States

[§]Chemical Science and Engineering Division, Advanced Photon Source, Argonne National Laboratory, 9700 South Cass Avenue, Argonne, Illinois 60439, United States

[∥]School of Chemical Engineering, Purdue University, 480 Stadium Mall Drive, West Lafayette, Indiana 47907-2100,United States

[⊥]Institute for Integrated Catalysis, Pacific Northwest National Laboratory, P.O. Box 999, Richland, Washington 99352, United States

[#]Department of Chemistry and Catalysis Research Institute, Technische Universität München, Lichtenbergstrasse 4, 85748 Garching, Germany

[¶]Department of Chemistry, Faculty of Science, King Abdulaziz University, Jeddah 21589, Saudi Arabia

Supporting Information

ABSTRACT: Developing supported single-site catalysts is an important goal in heterogeneous catalysis since the well-defined active sites afford opportunities for detailed mechanistic studies, thereby facilitating the design of improved catalysts. We present herein a method for installing Ni ions uniformly and precisely on the node of a Zr-based metal–organic framework (MOF), NU-1000, in high density and large quantity (denoted as Ni-AIM) using atomic layer deposition (ALD) in a MOF (AIM). Ni-AIM is demonstrated to be an efficient gas-phase hydrogenation catalyst upon activation. The structure of the active sites in Ni-AIM is proposed, revealing its single-site nature. More importantly, due to the organic linker used to construct the MOF support, the Ni ions stay isolated throughout the hydrogenation catalysis, in accord with its long-term stability. A quantum chemical characterization of the catalyst and the catalytic process complements the experimental results. With validation of computational modeling protocols, we further targeted ethylene oligomerization catalysis by Ni-AIM guided by theoretical prediction. Given the generality of the AIM methodology, this emerging class of materials should prove ripe for the discovery of new catalysts for the transformation of volatile substrates.

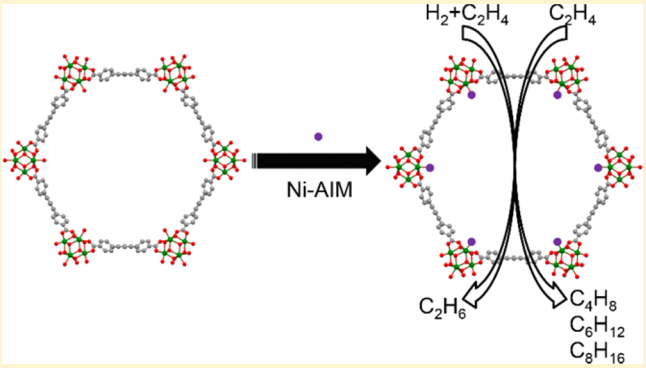

INTRODUCTION

Supported catalysts, composed of small metal/metal-oxide crystallites well dispersed on porous solid materials, play essential roles in a plethora of industrial gas-phase catalytic reactions including steam reforming, Fischer–Tropsch, and Haber–Bosch processes.[1−3] Solid supports such as porous activated carbon[4] or zeolites[5] are commonly used to increase the number, and/or enhance the activity ("support effects"), of candidate catalysis sites thereby boosting the overall efficiency of a catalyst.[3] As compared to conventional supports, the structures of MOFs,[6−9] a class of porous materials comprised of organic linkers and inorganic nodes, are more readily tuned by rational ligand design, as evidenced by the vast number of unique structures[10] and by wide potential for applications in gas storage[11] and separation,[12] chemical sensing,[13] and catalysis.[14,15] Furthermore, using crystalline MOFs as supports provides opportunities for atomically precise structural characterization of both active sites and supports, thereby facilitating detailed mechanistic studies of reactions.[16]

Appropriately designed Zr-based MOFs hold great potential for use as solid supports in gas-phase catalysis due to their

Received: November 30, 2015
Published: February 2, 2016

DOI: 10.1021/jacs.5b12515
J. Am. Chem. Soc. 2016, 138, 1977−1982

extraordinary thermal and chemical stabilities, as well as their substantial internal surface areas.[17] More importantly, it has been shown that these MOFs are readily modified post-synthetically to impart novel properties.[18] These functionalization processes, however, usually occur in solution phase, requiring laborious experimental procedures to remove trapped reagents and/or solvent.[18] Under certain circumstances, the ligation of solvent molecules to the coordinatively unsaturated metal sites can lead to a distinct reduction in, or even a complete loss of, the desired functionalities,[19] necessitating delivery of modifying agents via the vapor phase. In fact, early reports demonstrated that a few "metal@MOF" materials could be obtained by using volatile metal complexes under sublimation-like conditions.[20] However, the lack of specific metal attachment sites in these MOFs, together with the non-self-limiting nature of sublimation, precludes precise control of the metal distribution within the frameworks and results in unstable and/or poorly defined hybrid materials. Thus, the metal atoms in these materials often agglomerate, leading to a reduction in the number of active sites and corresponding loss of catalytic activity.[20] With these challenges in mind, we set out to use atomic layer deposition in MOF, or AIM to incorporate catalytic metal oxides in a site-specific and atomically controlled fashion.[21] More critically, by isolating support sites from each other via lengthy organic spacers, we aimed to preclude metal atom/ion migration and catalyst sintering—an all too common mode of deactivation of metal catalysts on conventional supports, especially when the catalysis occurs at elevated temperatures and under a reducing environment.[1]

NU-1000, composed of $Zr_6(\mu_3\text{-}O)_4(\mu_3\text{-}OH)_4(H_2O)_4(OH)_4$ nodes and tetratopic 1,3,6,8-(*p*-benzoate)pyrene ($TBAPy^{4-}$) linkers, makes an excellent platform for AIM studies due to the readily accessible $-OH/-OH_2$ groups on the Zr_6 nodes (Figure 1).[22] We have previously demonstrated that the

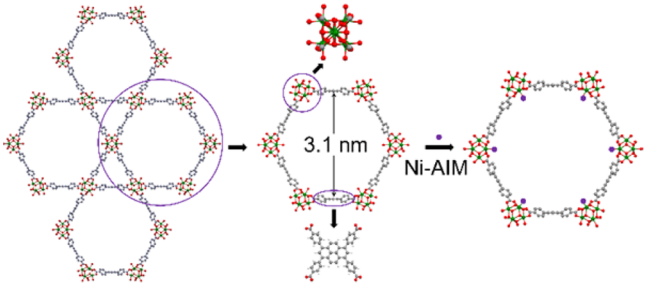

Figure 1. Structural representation of NU-1000, highlighting its organic linker, mesoporous channel, and Zr_6-containing node and a schematic depiction of the process used to anchor Ni to the Zr_6 node of NU-1000 via AIM. Color code: Zr (green), O (red), C (gray), H (white), Ni (purple).

structurally well-defined $-OH/-OH_2$ groups on Zr_6 nodes[23] can behave as site-isolating grafting sites to control the positions of deposited metal ions.[24] Our target metal was nickel as it exhibits excellent catalytic activity for gas-phase alkene hydrogenation/oligomerization when dispersed on porous platforms.[25] In this report, we first detail our investigations on ethylene hydrogenation catalyzed by Ni-AIM as a proof-of-concept reaction to (i) demonstrate that AIM affords an effective strategy in producing single-site catalysts and circumvents active-site sintering during catalysis and (ii) validate our computational modeling protocols for this new class of catalysts. Guided by theoretical predictions, we further investigated the potential of Ni-AIM for ethylene oligomerization, and our preliminary experimental results in this aspect are also presented herein.

RESULTS AND DISCUSSION

The synthesis and characterization of Ni-AIM are detailed in the Methods section and Supporting Information (SI). The as-synthesized material showed negligible ethylene hydrogenation activity over a temperature range of 50−200 °C. However, pretreatment in flowing 3% H_2/Ar at 200 °C renders the material catalytically active, with a per-nickel-atom turnover frequency (TOF) for ethylene hydrogenation of 0.9 ± 0.3 s^{-1} (Figure 2a). Notably, Ni-AIM is highly stable; e.g., with an

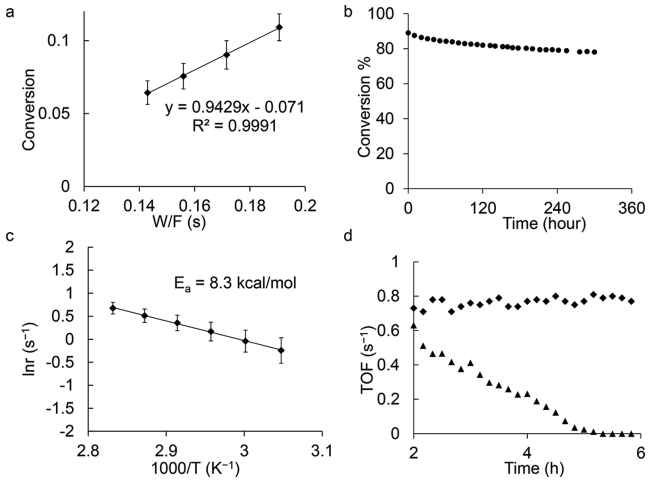

Figure 2. Catalytic conversion of ethylene to ethane. (a) TOF of the hydrogenation of ethylene catalyzed by activated Ni-AIM. (b) Stability test of activated Ni-AIM with initial 90% ethylene conversion. (c) Arrhenius plot of ethylene hydrogenation reaction rates by activated Ni-AIM. (d) Comparison of TOFs for Ni-AIM (diamond) and Ni-ZrO_2 (triangle).

initial ∼90% ethylene conversion, the deactivation of Ni-AIM was demonstrated to be minimal after 2 weeks' time on stream, reaching a final steady state conversion of ∼80% (Figure 2b). Additionally, with only 68 mg of material, ongoing 100% ethylene conversion (flow conditions) was observed for 2 weeks with no detectable loss of activity. Exposing the catalyst to ambient atmosphere causes complete deactivation; however, the catalytic activity was fully restored by repeating the H_2 pretreatment at 200 °C for 5 h (Figure S1). The apparent activation barrier of the reaction was 8.3 ± 1.4 kcal/mol (Figure 2c), similar to other reported hydrogenation catalysts.[26] For comparison, a commercial Pt catalyst supported on alumina (5 wt %, 40% dispersion) and a lab-synthesized catalyst, Ni-ZrO_2, were tested under the same conditions. Being 4 orders of magnitude more expensive than nickel, the platinum catalyst has a TOF of 35 ± 8 s^{-1}. Prepared by ALD, Ni-ZrO_2 had an initial TOF of 0.6 s^{-1} but quickly and irreversibly deactivated (Figure 2d). The observed decay is a striking, but hardly atypical illustration of catalytically debilitating consequences of active-site migration and sintering. The hexazirconium(IV)-oxo, hydroxo nodes of NU-1000 present a chemically similar environment/support but with migration and sintering systematically blocked by organic linkers/spacers of about nanometer dimensions. The practical manifestation of blocking is the contrasting persistence of high catalytic activity illustrated in

DOI: 10.1021/jacs.5b12515
J. Am. Chem. Soc. 2016, 138, 1977−1982

the panels b and d of Figure 2. Additionally, it was found that Ni-SiO_2 (preparation method is detailed in SI) consists mainly of NiO particles (Figure S3), illustrating the difficulty in producing site-isolated catalysts, especially with a high density of active sites. Moreover, a higher temperature (400 °C) is required for its activation, under which circumstances the material became black in color, indicative of Ni nanoparticle formation. This is in line with the previous reports that metallic Ni supported on silica[27] and zeolites[28] is active for hydrogenation reactions but only after activation at high temperatures.

In situ X-ray absorption spectroscopy experiments were performed to investigate the electronic and geometric structure of the Ni-AIM sites before and after activation with H_2 at 200 °C. X-ray absorption near edge structure (XANES) assessments of both the as-synthesized and activated Ni-AIM (Figure S2a) point to the retention of the Ni(II) oxidation state after the activation. We also observe a minor increase in XANES intensity ~8342 eV upon activation corresponding to the region of the 1s−4p electronic transition. Overall the pre-edge region indicates that the majority of Ni species in the catalyst retains the original symmetry upon activation. From extended X-ray absorption fine structure (EXAFS) spectra, we observe that upon activation the intensity of the peak at a phase uncorrected distance of ~1.6 Å (Ni−O scattering path) decreased, and its position shifted slightly (Figure 3a and

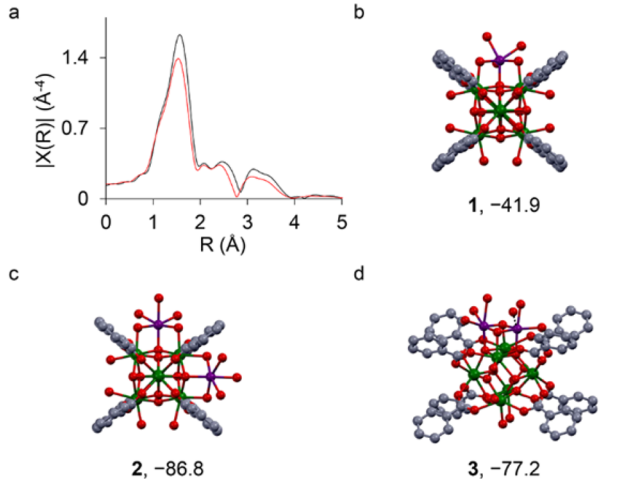

Figure 3. (a) EXAFS spectra of Ni-AIM before (black) and after (red) activation in 3% H_2/N_2 at 200 °C for 2 h; DFT calculated node structure for (b) one Ni atom per face model with one Ni atom included (−41.9 kcal/mol), (c) one Ni atom per face model with two Ni atoms included (−86.8 kcal/mol), and (d) two Ni atoms per face model (−77.2 kcal/mol). The enthalpies are relative to the reactants, i.e., bare NU-1000 node, two $Ni(MeC(Nt\text{-}Bu)_2)_2$, and six water molecules.

Figure S2b). Fitting this peak suggests a decrease of the average Ni first shell coordination number from 5.4 ± 0.6 to 5.0 ± 0.5. This decrease is accompanied by a decrease of the average Ni−O first shell bond distance from 2.056 and 2.033 Å (Figures S3−S5, Table S1). Both the XANES and the EXAFS results suggest some structural change upon activation—one consistent, as discussed below, with the formation of a small fraction of Ni hydride. EXAFS suggests that under reaction conditions this species likely exists as a transient state rather than a stable initial state.

Density functional theory (DFT) calculations were conducted to elucidate the reaction pathway of the Ni-AIM process (for details, see SI, Figure S6). Given the experimental observation of four Ni atoms per Zr_6 node, we first examined the energetics of depositing one Ni atom at the node (**1**, Movie S1) and then subsequently the energetics of depositing a second Ni atom at either another face of the node (**2**, Movie S2) or the same face as the first Ni atom (**3**, Movie S3). As shown in Figure 3, deposition of Ni atoms on separate faces is energetically (computationally) preferred by ~10 kcal/mol. Two factors likely contribute to this energy difference: (i) removal of a proton from the μ_3-OH group to permit formation of a μ_3-O−Ni bond renders **1** the most stable structure for single-Ni tautomers, but each face presents only one μ_3-OH group, and (ii) depositing two Ni atoms on the same node face involves using the node μ_3-O atom on that face as a ligand to nickel—the μ_3-O atom is slightly displaced toward the center of the node core compared to the sitting of the μ_3-OH group (which is deprotonated to serve as a ligand to the first deposited Ni atom). Coordination of the second Ni atom to the inwardly displaced μ_3-O is sufficiently sterically demanding such that one external water ligand moves from the inner coordination sphere of the second Ni into the second solvation shell, and this reduces the overall stability of the single-face dimer. Hence the isolated Ni model is used for DFT calculations of a plausible reaction energy pathway. Modeling the Ni atoms on separate faces allows for a direct evaluation of any cooperativity associated with the presence of the second metal. As the exothermicity required to deposit one Ni atom (−41.9 kcal/mol) is approximately half of that for the deposition of two adjacent Ni atoms (−86.8 kcal/mol), we conclude there is little communication between the faces, a situation similar to predictions for AIM reactions of NU-1000 nodes with Group 13 ALD precursors.[24]

The mechanism for catalytic ethylene hydrogenation was subsequently investigated using the calculated species **1** (Figure 4). We predict that one −OH equivalent is protonated by H_2 and departs as water during the activation process, leaving a hydride in its place (Figure S7). The transition-state structure we identified, involving the reaction of H_2 with yet another tautomer, **4**, generates **5** and has a fairly high enthalpy (43.2 kcal/mol), consistent with the overall strongly endothermic nature of the reaction, and rationalizes the forcing conditions associated with Ni-AIM activation.[29]

Upon activation, the complex binds one ethylene molecule to generate **6** from **5** with concomitant loss of two water molecules, which is predicted to be endothermic by 15 kcal/mol (but is strongly favorable in a free-energy sense under conditions that remove the water). Subsequent migratory insertion to generate the ethyl-nickel species **7** occurs with a low activation enthalpy of 3.7 kcal/mol and is exothermic by 12.0 kcal/mol once the initial loss of water ligands occurs. Subsequent binding of H_2 to **7** generates **8**, which then reacts to liberate ethane and generate the 4-coordinate nickel hydride species **9** with an activation enthalpy of 4.1 kcal/mol relative to **7** and an exothermicity of 4.9 kcal/mol. It is unclear whether this portion of the catalytic reaction is stepwise or concerted. While **8** exists as a minimum on the potential energy surface, the loss of zero-point vibrational energy associated with the binding of H_2 places **8** slightly higher in enthalpy than **7**. From an enthalpic standpoint, one might consider the production of ethane to proceed via the direct route from **7** to **9**. Nonetheless, both reaction pathways are predicted to proceed with very low

DOI: 10.1021/jacs.5b12515
J. Am. Chem. Soc. 2016, 138, 1977−1982

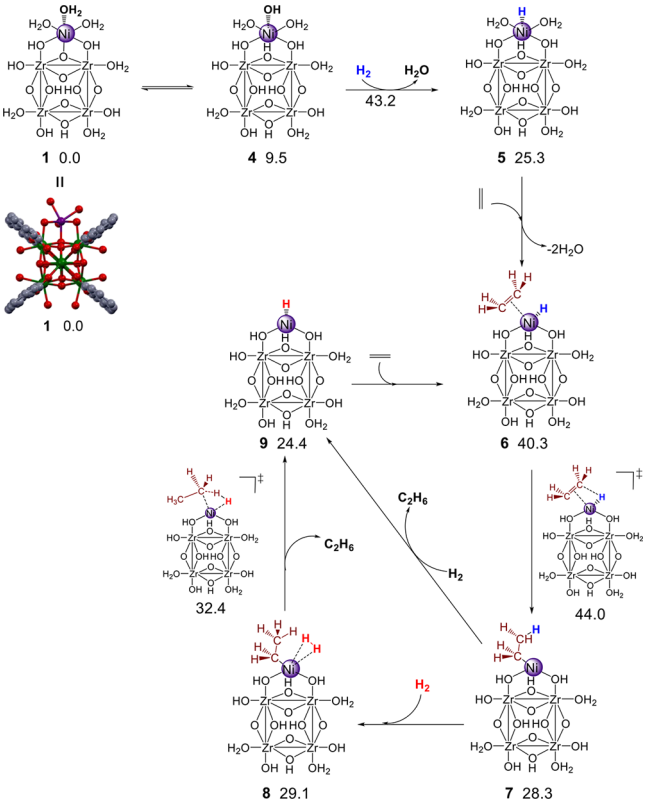

Figure 4. DFT-calculated enthalpies (kcal/mol relative to each reactant, i.e., **1**, 2 H_2, and $H_2C{=}CH_2$) for intermediates and transition state structures associated with Ni activation and single-turnover catalytic hydrogenation of ethylene (simplified for one Ni per node). For clarity, the benzoate ligands and the apical Zr atoms of the MOF are not shown.

activation enthalpies, leading to a very efficient catalytic cycle (Figure 4). Including a factor of RT at 373 K to convert an enthalpy of activation to an Arrhenius activation energy, the predicted value of 4.9 kcal/mol for the rate-determining step is slightly below the lower error bar on the measured value (*vide supra*), but we deem the agreement satisfactory given the limitations associated with modeling the MOF as a truncated cluster. We note, however, that while the Ni-AIM structure predicted from DFT calculations is consistent with the observed chemistry exploring other possible Ni-coordination motifs that may have similar energy minima is currently an active area of theoretical and experimental research.

The prediction of a Ni−H species in the hydrogenation process prompts us to target the ethylene oligomerization reaction as this intermediate is also involved in the mechanistic step for Ni-catalyzed alkene oligomerization.[30] Developing light alkene oligomerization catalysts has attracted tremendous industrial and academic interest in recent years since high-valued hydrocarbons such as gasoline, diesel fuel, lubricants, and surfactants can be produced via this process.[25] By the addition of $(CH_3CH_2)_2AlCl$, Ni-AIM becomes active for ethylene oligomerization at 45 °C and 2 bar pressure, with an estimated initial TOF of 0.3 s^{-1}. During the first 10 h on stream the catalyst deactivates, which is attributed to the formation of polymeric products (*vide infra*). Thereafter, a constant ethylene conversion is observed with the products being C_4, C_6, and C_8 (for product distributions, see Table S2). A series of detailed kinetics measurements were conducted in a similar fashion to the hydrogenation process, revealing a TOF of 0.07 ± 0.01 s^{-1} and an activation barrier of 8.5 kcal/mol (Figure 5), outperforming another reported MOF-based alkene oligomerization catalyst.[31]

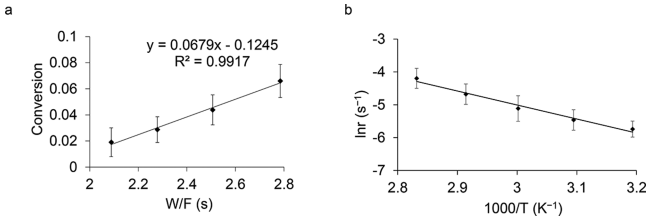

Figure 5. Catalytic conversion of ethylene oligomerization. (a) TOF of the oligomerization of ethylene catalyzed by activated Ni-AIM. (b) Arrhenius plot of ethylene oligomerization reaction rates by activated Ni-AIM.

CONCLUSION

With high activity, long-term stability, and excellent regenerability, the Ni-AIM material presented is one of the best available hydrogenation catalysts based on earth-abundant elements. Detailed structural analysis confirms that AIM affords an effective strategy to produce stable single-site catalysts because (i) there are strong interactions between the deposited metal ions and the Zr_6 node and (ii) the organic ligands that are used to construct the MOF can prevent the metal ions from migration and agglomeration. In addition, the molecular nature of the MOF support allows for the detailed characterization of the catalyst, providing a convenient platform for detailed mechanistic investigations of the catalytic cycle computationally. Of greater interest, with the validation of computational modeling protocols by the hydrogenation process, we successfully predicted and achieved the oligomerization process catalyzed by Ni-AIM. Further efforts involving the detailed mechanistic study of the oligomerization reaction are currently in progress.

METHODS

The parent MOF, NU-1000, was synthesized through a slightly modified literature procedure and is detailed in the Supporting Information. Upon activation, the integrity and quality of the obtained material is confirmed by N_2 isotherm measurements and powder X-ray diffraction (PXRD). For the AIM process, the compound bis(*N*,*N*′-di-*tert*-butyl-acetamidinato)nickel(II), $Ni(MeC(Nt\text{-}Bu)_2)_2$ (reactant A, Figure S8), was chosen as the Ni precursor due to its high thermal stability and its high volatility at relatively low temperature.[32] Room-temperature deionized H_2O is used as a coreactant to form NiO(H) on the Zr_6 nodes. In a typical experiment, a custom-made stainless steel powder sample holder containing microcrystalline NU-1000 (60.0 mg, 0.028 mmol) was placed in the ALD chamber, which was held at 125 °C for 30 min to remove physisorbed water before dosing with the Ni precursor. A cylinder containing $Ni(MeC(Nt\text{-}Bu)_2)_2$ is held at 120 °C, and each of its pulses follows the time sequence of t_1−t_2−t_3, where t_1 is the precursor pulse time, t_2 the exposure time, and t_3 the N_2 purge time (t_1 = 1 s, t_2 = t_3 = 300 s). To ensure full metalation of the Zr_6 sites throughout the microcrystals, the $Ni(MeC(Nt\text{-}Bu)_2)_2$ pulsing cycle was run 100× before subjecting the MOF to H_2O pulses.

Retention of crystallinity in Ni-AIM is confirmed by both scanning electron microscopy (SEM) and PXRD (Figure S9). Brunauer−Emmett−Teller (BET) analysis of the N_2 isotherms of an activated Ni-AIM sample (120 °C, evacuated for 12 h) indicates a surface area decrease from 2300 to 1450 $m^2{\cdot}g^{-1}$ as compared to undecorated NU-1000, in line with installation of Ni ions in the MOF crystallites and

DOI: 10.1021/jacs.5b12515
J. Am. Chem. Soc. 2016, 138, 1977−1982

with our previous work (Figure S10).[22,33] DFT-analyzed pore-size distributions show a corresponding decrease in the diameter of the hexagonal pores from 31 to 27 Å (Figure S10). The presence of Ni in Ni-AIM is confirmed by X-ray photoelectron spectroscopy (XPS), from which we can clearly observe at 856.5 eV a peak due to the $2p_{3/2}$ electrons of Ni(II) (Figure S11). Conformal deposition of Ni(II) within NU-1000 microcrystals was demonstrated via scanning electron microscopy−energy-dispersive X-ray spectroscopy. As displayed in Figure S11, along with the trace for Zr in Ni-AIM, a trace accounting for Ni is observed through the entire crystal with constant intensity when scanning the microcrystals of Ni-AIM through both dimensions. From inductively coupled plasma−atomic emission spectroscopy (ICP−AES) measurements of digested samples, the Ni content was consistently found to be 4.1 ± 0.4 Ni atoms per Zr_6 node. More pulses of the Ni precursor did not yield significant additional metal loading, consistent with the expected self-limiting behavior of the AIM process. In diffuse reflectance infrared Fourier transform spectra (DRIFTS), a significant decrease in the intensity of the peak centering around 3674 cm^{-1} was observed for the Ni-AIM material, suggesting that metalation occurs at the $-H_2O$ and $-OH$ sites of the Zr_6 node. The disappearance of the peaks at ∼2745, 2747, and 2551 cm^{-1} in the DRIFTS of Ni-AIM, attributed to the hydrogen-bonded $-OH/-H_2O$ stretching frequency in NU-1000, further corroborates metalation at the Zr_6 nodes (Figure S12). Thermal gravimetric analysis of Ni-AIM yielded little mass loss up to 300 °C, indicative of the catalyst's good thermal stability (Figure S13).

Ni-AIM is converted to its catalytically active form by exposure to flowing 3% H_2 (200 mL/min; 1.5 bar total pressure) at 200 °C for 2 h. For example, following activation of Ni-AIM (40 mg), 100% ethylene conversion is observed at 100 °C, while no conversion occurs with the as-synthesized Ni-AIM. For kinetic studies (Ni-AIM, Pt@alumina, and Ni-ZrO_2), the gas-flow ratio for ethylene:H_2 was set to 1:2, and catalysis was studied at 50 °C, 1.5 bar total pressure. For catalyst stability tests of Ni-AIM, experiments were conducted at 100 °C, 1.5 bar total pressure, with 40 mL/min ethylene, 80 mL/min H_2, and 120 mL/min N_2.

After the catalysis, the recovered Ni-AIM was subjected to further scrutiny by PXRD, SEM (Figure S14 for hydrogenation and Figure S15 for the oligomerization); no evidence for Ni sintering or agglomeration and no evidence for loss of framework crystallinity were found. Comparison between the EXAFS spectra of Ni-AIM before and after hydrogenation catalysis is displayed in Figure S14d, and the minimal change between them indicates the high stability of the Ni-AIM material. ICP−AES analysis revealed no detectable change in Ni content, i.e., no evidence for loss during catalytic runs. For a Ni-AIM sample recovered after 1 day's hydrogenation catalysis a BET surface area of 1150 $m^2 \cdot g^{-1}$ was obtained—slightly lower than before use as a catalyst. (We cannot rule out post-catalysis contamination of the sample with quartz wool from the reactor as an explanation for the apparent reduction in gravimetric area.)

■ ASSOCIATED CONTENT

Supporting Information

The Supporting Information is available free of charge on the ACS Publications website at DOI: 10.1021/jacs.5b12515.

Addition materials synthesis and characterization data and computational details (PDF)
Detailed structure representation of **1** (AVI)
Detailed structure representation of **2** (AVI)
Detailed structure representation of **3** (AVI)

■ AUTHOR INFORMATION

Corresponding Authors

*C.J.C. (cramer@umn.edu).
*L.G. (gagliard@umn.edu).
*J.T.H. (j-hupp@northwestern.edu).
*O.K.F (o-farha@northwestern.edu).

Author Contributions

The manuscript was written through contributions of all authors. All authors have given approval to the final version of the manuscript.

Notes

The authors declare no competing financial interest.

■ ACKNOWLEDGMENTS

O.K.F., J.T.H., C.J.C., and L.G. gratefully acknowledge the financial support from the Inorganometallic Catalyst Design Center, an EFRC funded by the DOE, Office of Basic Energy Sciences (DE-SC0012702). A.V., J.L.F. and J.A.L gratefully acknowledge the financial support from the Inorganometallic Catalyst Design Center, an EFRC funded by the DOE, Office of Basic Energy Sciences (DE-SC0012702). The work was performed at the Pacific Northwest National Laboratory operated by Battelle for the U.S. Department of Energy. A.W.P was supported by the Department of Defense (DoD) through the National Defense Science and Engineering Fellowship (NDSEG) program. JTM and AG Getsoian were supported by the U.S. Department of Energy, Office of Basic Energy Sciences, Chemical Sciences under Contract DE-AC-02-06CH11357. This work made use of the J.B. Cohen X-ray Diffraction Facility supported by the MRSEC program of the National Science Foundation (DMR-1121262) at the Materials Research Center of Northwestern University. This work made use of the EPIC facility (NUANCE Center-Northwestern University), which has received support from the MRSEC program (NSF DMR-1121262) at the Materials Research Center; the International Institute for Nanotechnology (IIN); and the State of Illinois, through the IIN. This work made use of IMSERC facilities at Northwestern University supported by the National Institutes of Health under NIH (1S10OD012016-01/1S10RR019071-01A1). Use of the Advanced Photon Source is supported by the U.S. Department of Energy, Office of Science, and Office of Basic Energy Sciences, under Contract DE-AC02-06CH11357. Materials Research Collaborative Access Team (MRCAT, Sectors 10 μ_B and 10ID) operations are supported by the Department of Energy and the MRCAT member institutions.

■ REFERENCES

(1) Flytzani-Stephanopoulos, M.; Gates, B. C. *Annu. Rev. Chem. Biomol. Eng.* **2012**, *3*, 545−574.
(2) Thomas, J. M.; Raja, R.; Lewis, D. W. *Angew. Chem., Int. Ed.* **2005**, *44*, 6456−6482.
(3) Deutschmann, O.; Knözinger, H.; Kochloefl, K.; Turek, T. Heterogeneous catalysis and solid catalysts, 2. development and types of solid catalysts. *Ullmann's Encyclopedia of Industrial Chemistry*; Wiley-VCH Verlag GmbH & Co. KGaA: Weinheim, 2012.
(4) Jüntgen, H. *Fuel* **1983**, *65*, 1436−1446.
(5) Davis, R. J. *J. Catal.* **2003**, *216*, 396−405.
(6) Yaghi, O. M.; O'Keeffe, M.; Ockwig, N. W.; Chae, H. K.; Eddaoudi, M.; Kim, J. *Nature* **2003**, *423*, 705−714.
(7) Horike, S.; Shimomura, S.; Kitagawa, S. *Nat. Chem.* **2009**, *1*, 695−704.
(8) Eddaoudi, M.; Sava, D. F.; Eubank, J. F.; Adil, K.; Guillerm, V. *Chem. Soc. Rev.* **2015**, *44*, 228−249.
(9) Ferey, G. *Chem. Soc. Rev.* **2008**, *37*, 191−214.
(10) Furukawa, H.; Cordova, K. E.; O'Keeffe, M.; Yaghi, O. M. *Science* **2013**, *341*, 974−986.
(11) Murray, L. J.; Dinca, M.; Long, J. R. *Chem. Soc. Rev.* **2009**, *38*, 1294−1314.

DOI: 10.1021/jacs.5b12515
J. Am. Chem. Soc. 2016, 138, 1977−1982

(12) McDonald, T. M.; Mason, J. A.; Kong, X.; Bloch, E. D.; Gygi, D.; Dani, A.; Crocella, V.; Giordanino, F.; Odoh, S. O.; Drisdell, W.; Vlaisavljevich, B.; Dzubak, A. L.; Poloni, R.; Schnell, S. K.; Planas, N.; Lee, K.; Pascal, T.; Wan, L. F.; Prendergast, D.; Neaton, J. B.; Smit, B.; Kortright, J. B.; Gagliardi, L.; Bordiga, S.; Reimer, J. A.; Long, J. R. *Nature* **2015**, *519*, 303−308.
(13) Kreno, L. E.; Leong, K.; Farha, O. K.; Allendorf, M.; Van Duyne, R. P.; Hupp, J. T. *Chem. Rev.* **2012**, *112*, 1105−1125.
(14) Lee, J.; Farha, O. K.; Roberts, J.; Scheidt, K.; Nguyen, S. T.; Hupp, J. T. *Chem. Soc. Rev.* **2009**, *38*, 1450−1459.
(15) Ma, L. Q.; Abney, C.; Lin, W. *Chem. Soc. Rev.* **2009**, *38*, 1248−1256.
(16) Vermoortele, F.; Vandichel, M.; Van de Voorde, B.; Ameloot, R.; Waroquier, M.; Van Speybroeck, V.; De Vos, D. E. *Angew. Chem., Int. Ed.* **2012**, *51*, 4887−4890.
(17) Howarth, A. J.; Liu, Y.; Li, P.; Li, Z.; Wang, T. C.; Hupp, J. T.; Farha, O. K. *Nat. Rev. Mater.* **2016**, DOI: 10.1038/natrevmats.2015.18.
(18) Deria, P.; Mondloch, J. E.; Karagiaridi, O.; Bury, W.; Hupp, J. T.; Farha, O. K. *Chem. Soc. Rev.* **2014**, *43*, 5896−5912.
(19) Sumida, K.; Stück, D.; Mino, L.; Chai, J.-D.; Bloch, E.; Zavorotynska, O.; Murray, L.; Dinca, M.; Chavan, S.; Bordiga, S.; Head-Gordon, M.; Long, J. *J. Am. Chem. Soc.* **2013**, *135*, 1083−1091.
(20) Meilikhov, M.; Yusenko, K.; Esken, D.; Turner, S.; Van Tendeloo, G.; Fischer, R. A. *Eur. J. Inorg. Chem.* **2010**, *24*, 3701−3714.
(21) George, S. M. *Chem. Rev.* **2010**, *110*, 111−131.
(22) Mondloch, J. E.; Bury, W.; Fairen-Jimenez, D.; Kwon, S.; DeMarco, E. J.; Weston, M. H.; Sarjeant, A. A.; Nguyen, S. T.; Stair, P. C.; Snurr, R. Q.; Farha, O. K.; Hupp, J. T. *J. Am. Chem. Soc.* **2013**, *135*, 10294−10297.
(23) Planas, N.; Mondloch, J. E.; Tussupbayev, S.; Borycz, J.; Gagliardi, L.; Hupp, J. T.; Farha, O. K.; Cramer, C. J. *J. Phys. Chem. Lett.* **2014**, *5*, 3716−3723.
(24) Kim, I. S.; Borycz, J.; Platero-Prats, A. E.; Tussupbayev, S.; Wang, T. C.; Farha, O. K.; Hupp, J. T.; Gagliardi, L.; Chapman, K. W.; Cramer, C. J.; Martinson, A. B. F. *Chem. Mater.* **2015**, *27*, 4772−4778.
(25) Finiels, A.; Fajula, F.; Hulea, V. *Catal. Sci. Technol.* **2014**, *4*, 2412−2426.
(26) Somorjai, G. A.; Li, Y. *Introduction to Surface Chemistry and Catalysis*; John Wiley & Sons, Inc.: Hoboken: New Jersey, 2010.
(27) Koh, H.; Hughes, R. *J. Catal.* **1974**, *33*, 7−16.
(28) Suzuki, M.; Tsutsumi, K.; Takahashi, H. *Zeolites* **1982**, *2*, 185−192.
(29) Andreasen, A. *Predicting Formation Enthalpies of Metal Hydrides*; Pitney Bowes Management Services: Roskilde, 2004.
(30) Speiser, F.; Braunstein, P.; Saussine, L. *Acc. Chem. Res.* **2005**, *38*, 784−793.
(31) Mlinar, A. N.; Keitz, B. K.; Gygi, D.; Bloch, E. D.; Long, J. R.; Bell, A. T. *ACS Catal.* **2014**, *4*, 717−721.
(32) Lim, B. S.; Rahtu, A.; Gordon, R. G. *Nat. Mater.* **2003**, *2*, 749−754.
(33) Peters, A. W.; Li, Z.; Farha, O. K.; Hupp, J. T. *ACS Nano* **2015**, *9* (8), 8484−8490.

DOI: 10.1021/jacs.5b12515
J. Am. Chem. Soc. 2016, 138, 1977−1982